U. S. Naval Research Laboratory
Washington, DC 20375-5320

NRL/7130/FR--2021/1

Far-Field Pressures from Doubly Periodic Three-Dimensional Elastic Panels

Mauricio Villa
Saikat Dey
David Raudales
Zachary Waters
Physical Acoustics Branch, Acoustics Division
Naval Research Laboratory

May 3, 2021

REPORT DOCUMENTATION PAGE

Form Approved
OMB No. 0704-0188

1. REPORT DATE (DD-MM-YYYY)	2. REPORT TYPE	3. DATES COVERED (From – To)
28-04-2021	NRL Formal Report	June 2019 - May 2020

4. TITLE AND SUBTITLE

Far-Field Pressures from Doubly Periodic Three-Dimensional Elastic Panels

5a. CONTRACT NUMBER

5b. GRANT NUMBER

5c. PROGRAM ELEMENT NUMBER

6. AUTHOR(S)

Mauricio Villa, Saikat Dey, David Raudales, Zachary Waters

5d. PROJECT NUMBER

5e. TASK NUMBER

5f. WORK UNIT NUMBER
6B11

7. PERFORMING ORGANIZATION NAME(S) AND ADDRESS(ES)

U. S. Naval Research Laboratory
4555 Overlook Avenue, SW
Washington, DC 20375-5320

8. PERFORMING ORGANIZATION REPORT NUMBER

NRL/7130/FR--2021/1

9. SPONSORING / MONITORING AGENCY NAME(S) AND ADDRESS(ES)

Office of Naval Research
One Liberty Center
875 N. Randolph Street, Suite 1425
Arlington, VA 22203-1995

10. SPONSOR / MONITOR'S ACRONYM(S)
ONR

11. SPONSOR / MONITOR'S REPORT NUMBER(S)

12. DISTRIBUTION / AVAILABILITY STATEMENT
Distribution Statement A: Approved for public release. Distribution is unlimited.

13. SUPPLEMENTARY NOTES
Karles Fellowship

14. ABSTRACT

We present an analysis and algorithm to calculate the scattered and transmitted far-field pressures for fluid-loaded doubly periodic elastic panels forced by a planar acoustic wave at an arbitrary angle of incidence. The elastic panels are of infinite extent and can have complex internal structures. The fluid-loaded structural response of a single unit cell is determined using the STARS3D finite element solver with periodic boundary conditions and the use of perfectly matched layers (PML) for the truncation of the semi-infinite fluid domains. The far-field pressure is a posteriori calculated by projecting the transverse motion of the wet surface of the unit cell with a simple Fourier analysis. As a result of the infinite periodicity of the configuration, the far-field pressures are represented as a summation of the finite set of radiating modes. Radiation fields for single and multilayered elastic layers with and without internal structures are shown to agree with analytical and numerical solutions.

15. SUBJECT TERMS
doubly periodic, elastic panels, far-field pressure, fourier analysis, meta-material

16. SECURITY CLASSIFICATION OF:			17. LIMITATION OF ABSTRACT	18. NUMBER OF PAGES	19a. NAME OF RESPONSIBLE PERSON
a. REPORT	b. ABSTRACT	c. THIS PAGE			Mauricio Villa
U	U	U	UU	27	19b. TELEPHONE NUMBER *(Include area code)* 202-767-7427

Standard Form 298 (Rev. 8-98)
Prescribed by ANSI Std. Z39.18

This page intentionally left blank

CONTENTS

FIGURES

TABLES

This page intentionally left blank

EXECUTIVE SUMMARY

Using panels of viso-elastic (meta)materials alters the structural-acoustic response of fluid-loaded elastic structures. In order to achieve the desired response, one needs an ability to model accurately the transmission and reflection of incident acoustic waves on panel-like elastic structures, which typically have doubly periodic, lattice-like arrangements. While the reflected and transmitted pressure fields can be computed close to the panels themselves using first-principles-based numerical techniques, they are prohibitively expensive to determine the *far-field* response. One needs a capability to project the *near-field* values in a range-independent manner to obtain the *far-field* response.

In this report, we describe a new theory based on *Fourier analysis* combined with first-principles-based numerical procedures for the projection of sound pressure reflected by and transmitted through doubly periodic elastic panels with complex internal structures has been developed.

The theory and its numerical implementation are verified for a sequence of increasingly complex doubly periodic panel configurations.

This page intentionally left blank

FAR-FIELD PRESSURES FROM DOUBLY PERIODIC THREE-DIMENSIONAL ELASTIC PANELS

1. INTRODUCTION

The structural-acoustic response of complex (visco)elastic panels subjected to incident acoustic waves has an important role in several applications. In the civilian realm, it helps in the design of effective noise abatement technologies for uses such as highway noise barriers and insulation layers for quieter aircraft and vehicle interiors. In the military realm, it helps reduce radiated and scattered noise from underwater elastic structures. In this regard, a lot of recent studies have focused on understanding and exploiting locally resonant structures [1] in lattice-like panels to produce continuum responses not observed in traditional materials. Material designed and engineered in this manner to manipulate the interaction of sound with structures is sometimes referred to as *meta-material* [2, 3]. Their continuum response manifests properties, such as negative stiffness and modulus, usually absent in naturally occurring materials.

The *near-field*[1] response of a periodic, lattice-like structure with complex geometry can be determined numerically using first-principles approaches coupled with appropriate periodic boundary conditions [4]. However, in many applications, one needs the *far-field* response, which is independent of the range of observation and only depends on the direction. In order to determine the far-field response, one theoretically can extend the domain of the numerical model to include the entire range of observations. In practice, this is not feasible due to the computationally large problem one must solve. Furthermore, it is not necessary to do this as one can use the asymptotic nature of the response that radiates to the far-field. When the panel is made of layers of homogeneous material, the near-field and far-field responses are identical by definition [5]. However, when the panel geometry is non-homogeneous, this is not the case and a method to project the range-dependent near-field response to a range-independent far-field is needed. In this work, we develop a theory and numerical algorithms to do this projection.

The rest of this report is structured as follows: Section 2 describes the model problem setup. Section 3 details the periodic boundary conditions needed due to lattice periodicity. Section 4 details the theory and numerical algorithms for the far-field projection, followed by numerical examples in Section 5 to verify the numerical procedures. Section 6 presents a summary and future work.

2. MODEL PROBLEM

Consider a semi-infinite panel along the xy plane with some finite thickness in z, as depicted in Fig. 1. The bounding fluid domains above and below the panel extend to infinity along the z-axis. We will consider the incident planar wave to originate from $z = +\infty$. The panel is considered to be periodic in both the x and y directions with periods L_x and L_y, respectively. Throughout this report, a single periodic element of dimensions L_x x L_y x L_z will be referred to as a unit cell. The unit cell can be homogeneous or can include structural inhomogeneities such as voids and internal elements with anisotropic material properties. We have

Manuscript approved May 3, 2021.

[1] Where the response is a function of the distance from the structure or range-dependent.

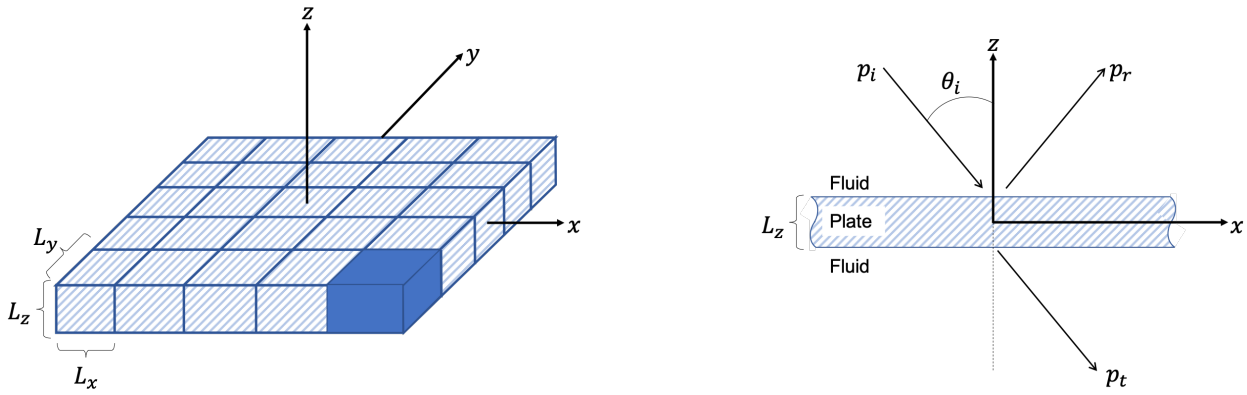

Fig. 1—Schematic of a unit cell (shaded) and the reference frame for the doubly-periodic plate

shown previously that the structural-acoustic response of a fluid-loaded periodic panel can be determined accurately with first principles combined with a perfectly matched layer (PML) formulation [4, 6]. With the use of periodic boundary conditions in the finite element analysis, only the geometry of a single elastic unit cell and the adjacent columns of fluid are modeled and meshed. The analysis allows for the efficient and accurate modeling of the near-field structural response of the insonified periodic panel. However, in order to determine the far-field pressures, the computational domain must be extended to include the far-field locations of interest, thus increasing the degrees of freedom and the computational cost of the numerical model. A projection of the evaluated transverse surface velocity of the unit cell is developed to describe the coupled far-field pressures, which is known as wave field extrapolation in Fourier acoustics [7]. This projection is contingent on the infinite periodicity of the panel, and as such, the periodicity conditions are discussed in the next section.

3. PERIODICITY CONDITIONS

The incident harmonic planar pressure wave p_i driving the panel is defined below, with the wavenumber components represented as functions of the three-dimensional angle of incidence θ_o and ϕ_o in the xz and yz planes, respectively

$$p_i(x, y, z, t) = P_o e^{i(k_{xo}x + k_{yo}y - k_{zo}z)} e^{-i\omega t} \tag{1a}$$

$$k_{xo} = k \sin\theta_o \cos\phi_o, \quad k_{yo} = k \sin\theta_o \sin\phi_o, \quad k_{zo} = k \cos\theta_o, \tag{1b}$$

where k is the acoustic wavenumber, ω is the angular driving frequency and c is the speed of sound of the fluid, all of which are related by

$$k = \frac{\omega}{c} = \frac{2\pi f}{c}, \tag{2}$$

Throughout the remainder of this document, the time harmonic dependence is assumed and omitted. It is convenient to define the phase function $\psi(x, y)$ to identify the influence of the planar wave obliqueness as

$$\psi(x, y) = e^{ik_{xo}x} e^{ik_{yo}y}, \tag{3}$$

The elastic velocity vector has three components, but for the current analysis, only the component normal to the plate surface $\dot{w}(x, y, z)$ is required. The periodicity of the panel response is defined such that the transverse velocity of the structure $\dot{w}(x, y, z)$ satisfies the condition

$$\dot{w}(x + N_x L_x, y + N_y L_y, z) = \dot{w}(x, y, z)\psi(N_x L_x, N_y L_y), \tag{4}$$

for indices $N_x, N_y = 0, \pm 1, \pm 2....$ That is, the velocity distributions of each of the cells differ only by a phase-shift that is defined by the angle of incidence and the excitation frequency of the incident pressure wave, which is a statement of the Bloch-Floquet Theorem [8]. For the special cases where at least one of the trace wavelength components is an integer multiple of the period lengths L_x, L_y, the phase function simplifies. The most restrictive periodicity condition occurs when the response of each unit cell of the plate is equivalent with no phase shift. That is

$$\psi(N_x L_x, N_y L_y) = 1 \tag{5a}$$

$$\dot{w}(x + N_x L_x, y + N_y L_y, z) = \dot{w}(x, y, z), \tag{5b}$$

In order for this periodicity condition to be satisfied for a given structural configuration (fixed L_x and L_y), the driving pressure wave is necessarily limited to a set of allowable incidence angles and driving frequencies. Consider the incident pressure p_i evaluated at the fluid-structure interface, which here is set to be at the $z = z_1$ plane. In order to satisfy the condition Eq. (5), the incident pressure has the corresponding condition

$$p_i(x + N_x L_x, y + N_y L_y, z_1) = p_i(x, y, z_1), \tag{6}$$

In order for this condition to be satisfied for all driving frequencies, the planar wave must be incident normal to the plate surface so that $\sin\theta_o = 0$.

4. ACOUSTIC FAR-FIELD PROJECTION

The following discussion considers the elastic unit cell located in the domain defined by $-L_x/2 \leq x \leq L_x/2$, $-L_y/2 \leq y \leq L_y/2$ and $-L_z/2 \leq z \leq L_z/2$, and it requires that the structural response of the unit cell due to the incident pressure wave in Eq. (1a) has been determined. Assuming that the elastic response for the single unit cell is known, only the normal component of the velocity at the fluid-structure interfaces is required to determine the coupled fluid pressures in the absence of viscous effects. These elastic surface velocities of the unit cell are denoted as $\dot{w}_c(x, y, z_j)$, where $z_j = \{z_1, z_2\}$ corresponds to the reflection and transmission surfaces, respectively. The general periodicity condition is applied to determine the normal surface velocities anywhere on the infinite panel $\dot{w}_s(x, y, z_i)$ as

$$\dot{w}_s(x + N_x L_x, y + N_y L_y, z_j) = \dot{w}_c(x, y, z_j)\psi(N_x L_x, N_y L_y), \tag{7}$$

The scattered $p_{sc}(x, y, z)$ and transmitted $p_t(x, y, z)$ pressures are determined readily by using the acoustic momentum equation to satisfy the boundary conditions normal to the plate at the corresponding structure-fluid interfaces:

$$\rho_f \frac{\partial \mathbf{v}}{\partial t} = -\nabla p, \tag{8}$$

where the subscript f corresponds to the fluid properties of the fluid domains above and below the panel. Satisfying the condition on the insonified surface, the gradient of the scattered pressure is evaluated as

$$\begin{aligned} \rho_f \frac{\partial}{\partial t}\dot{w}_s(x,y,z_1) &= -\frac{\partial}{\partial z}(p_{sc}(x,y,z_1) + p_i(x,y,z_1)) \\ \frac{\partial}{\partial z}p_{sc}(x,y,z_1) &= i\omega\rho_f \dot{w}_s(x,y,z_1) - \frac{\partial}{\partial z}p_i(x,y,z_1), \end{aligned} \tag{9}$$

The momentum balance is similar for the transmission side, with the absence of the incident pressure contribution,

$$\frac{\partial}{\partial z}p_t(x,y,z_2) = i\omega\rho_f \dot{w}_s(x,y,z_2). \tag{10}$$

4.1 Surface Velocity Eigenfunction Decomposition

A thorough development of Fourier analysis and its suitability to wave-field extrapolation is presented by Williams [7]. As a result of the infinitely periodic extent of the panel, the transverse surface velocities of the unit cell $\dot{w}_c(x,y,z_j)$ are expanded as a double Fourier series. To distinguish between the unit cell velocities and the resulting periodic extension defined by the Fourier series, we define $\dot{W}_c(x,y,z_j)$ to be the periodic extension of $\dot{w}_c(x,y,z_j)$ so that

$$\dot{W}_c(x,y,z_j) = \sum_{N_x=-\infty}^{+\infty}\sum_{N_y=-\infty}^{+\infty} \dot{W}_{j;N_x,N_y}\, e^{ik_{N_x}x} e^{ik_{N_y}y}, \tag{11a}$$

with Fourier components given by the eigenfunction projection that reduces to

$$\dot{W}_{j:N_x,N_y} = \frac{1}{L_x L_y}\int_{-L_x/2}^{L_x/2}\int_{-L_y/2}^{L_y/2} \dot{w}_c(x,y,z_j) e^{-ik_{N_x}x} e^{-ik_{N_y}y}\, dxdy, \tag{11b}$$

and the eigenvalues are given by

$$k_{N_x} = \frac{2\pi N_x}{L_x}, \qquad k_{N_y} = \frac{2\pi N_y}{L_y}, \tag{11c}$$

The decomposition of the unit cell surface velocity into the Fourier basis represents the velocity as the superposition of an infinite but discrete set of traveling waves with wavenumbers defined by the respective eigenvalues. Interpreting the eigenvalues as the trace wavenumbers of each individual wave, the wave propagation into the fluids is controlled by the resulting normal wavenumber component k_{N_z} which is defined below for completeness and will be discussed in Section 4.3:

$$k_{N_z} = \sqrt{k^2 - k_{N_x}^2 - k_{N_y}^2}. \tag{12}$$

The representation of the surface velocity could be treated just as well in the Fourier domain by application of the Fourier transform. In fact the Fourier transform would result in a description of the surface velocity as an appropriately scaled Dirac comb that is related to Eq. (11a) by the Poisson summation formula [7]. The Fourier series approach is used here for the physical interpretation it facilitates. Additionally, it will be shown that the Fourier series description lends itself to leverage existing *fast fourier transform* (FFT) implementations.

The periodic extension in Eq. (11a) would only represent the velocity of the infinite elastic media for the special case of normal incidence that satisfies the periodicity condition in Eq. (5). In order to generalize this result for oblique incidence, we rewrite the periodicity condition in Eq. (7), using the Bloch-Floquet Theorem, as the equivalent statement [8]

$$\dot{w}_s(x, y, z_j) = \dot{W}_c(x, y, z_j)\psi(x, y), \tag{13}$$

To demonstrate the equivalence of these statements of periodicity, we substitute $x' = x + N_x L_x$, $y' = y + N_y L_y$ and simplify to return the original condition of Eq. (4):

$$\begin{aligned}
\dot{w}_s(x', y', z_j) &= \dot{W}_c(x', y', z_j)\psi(x', y') \\
\dot{w}_s(x', y', z_j) &= \dot{W}_c(x, y, z_j)\psi(x, y)\psi(N_x L_x, N_y L_y) \\
\dot{w}_s(x + N_x L_x, y + N_y L_y, z_j) &= \dot{w}_s(x, y, z_j)\psi(N_x L_x, N_y L_y).
\end{aligned}$$

Returning to Eq. (13), the general Fourier series representation of the surface velocities of the periodic elastic domain are constructed with the harmonics defined below.

$$\dot{w}_s(x, y, z_j) = \sum_{N_x=-\infty}^{+\infty} \sum_{N_y=-\infty}^{+\infty} \dot{W}_{j;N_x,N_y}\, e^{i\bar{k}_{N_x} x} e^{i\bar{k}_{N_y} y} \tag{14a}$$

$$\bar{k}_{N_x} = \frac{2\pi N_x}{L_x} + k_{xo}, \qquad \bar{k}_{N_y} = \frac{2\pi N_y}{L_y} + k_{yo}, \qquad \bar{k}_{N_z} = \sqrt{k^2 - \bar{k}_{N_x}^2 - \bar{k}_{N_y}^2} \tag{14b}$$

$$\dot{W}_{j;N_x,N_y} = \frac{1}{L_x L_y} \int_{-L_x/2}^{L_x/2} \int_{-L_y/2}^{L_y/2} \dot{w}_s(x, y, z_j) e^{-i\bar{k}_{N_x} x} e^{-i\bar{k}_{N_y} y}\, dxdy \tag{14c}$$

This modified Fourier basis is sometimes referred to as space-harmonics [9, 10], where the modified eigenvalues of the space harmonics include the wavenumber information of the incident pressure. As a result of the bounds of integration in the definition for the modal amplitudes, Eq. (14c) can be rewritten using the known surface velocity of the unit cell at the origin. In order to leverage the definition and existing implementations of the Discrete Fourier Transform [7, 11], the modified eigenvalues are expanded so that

$$\dot{W}_{j;N_x,N_y} = \frac{1}{L_x L_y} \int_{-L_x/2}^{L_x/2} \int_{-L_y/2}^{L_y/2} \dot{w}_c(x, y, z_j)\overline{\psi(x, y)} e^{-ik_{N_x} x} e^{-ik_{N_y} y}\, dxdy, \tag{15}$$

where $\overline{\psi(x, y)}$ is the complex conjugate of the phase function. In practice, the velocity at each surface interface of the unit cell is evaluated at a grid of equally spaced discrete locations. Therefore, the discrete Fourier transform of $\dot{w}_c(x, y, z_j)\overline{\psi(x, y)}$ describes the modal amplitudes $\dot{W}_{j;N_x,N_y}$ to be used in Eq. (14a).

4.2 Pressure Fields Eigenfunction Decomposition

Like the surface velocity, the pressure components are expressed as double Fourier series representations such that

$$p_{sc}(x,y,z) = \sum_{N_x=-\infty}^{+\infty} \sum_{N_y=-\infty}^{+\infty} S_{N_x,N_y}\, e^{i\bar{k}_{N_x}x} e^{i\bar{k}_{N_y}y} e^{i\bar{k}_{N_z}z} \tag{16a}$$

$$p_t(x,y,z) = \sum_{N_x=-\infty}^{+\infty} \sum_{N_y=-\infty}^{+\infty} T_{N_x,N_y}\, e^{i\bar{k}_{N_x}x} e^{i\bar{k}_{N_y}y} e^{-i\bar{k}_{N_z}z} \tag{16b}$$

$$p_i(x,y,z) = \sum_{N_x=-\infty}^{+\infty} \sum_{N_y=-\infty}^{+\infty} P_{i_{N_x,N_y}}\, e^{i\bar{k}_{N_x}x} e^{i\bar{k}_{N_y}y} e^{-i\bar{k}_{N_z}z}, \tag{16c}$$

where the modal amplitudes S_{N_x,N_y} and T_{N_x,N_y} are the unknowns to be determined. The sign of the wavenumber component in the radiation direction $\bar{k}_{N_z}$ is chosen to satisfy the Sommerfeld radiation condition [7, 12]. Projecting the known incident pressure onto the eigenfunctions, the modal amplitudes are determined as

$$P_{i_{N_x,N_y}} e^{-i\bar{k}_{N_z}z} = \frac{P_o}{L_x L_y} \int_{-L_x/2}^{L_x/2} \int_{-L_y/2}^{L_y/2} \left[e^{i(k_{xo}x + k_{yo}y - k_{zo}z)} \right] e^{-i\bar{k}_{N_x}x} e^{-i\bar{k}_{N_y}y}\, dxdy. \tag{17}$$

As a result of orthogonality, the modal amplitudes of the incident pressure are only non-zero for $N_x = N_y = 0$. Recalling the definition of $\bar{k}_{N_z}$ in Eq. (14b), this simplifies Eq. (16c) to be identically Eq. (1a) as a result of the modal amplitude:

$$P_{i_{00}} = P_o e^{-ik_{zo}z} e^{i\bar{k}_{N_z}z}\Big|_{N_x=N_y=0} = P_o. \tag{18}$$

4.3 Evaluation of Pressure Fields

Finally, the series descriptions of the surface velocities and pressure components are substituted into the momentum equation Eq. (9) and Eq. (10) to determine the modal amplitudes of the pressure fields. The resulting modal amplitudes for the scattered and transmitted pressure fields are presented below. Again, note that the incident pressure only manifests in the scattered field amplitude, and only in the mode that physically represents specular reflection.

$$S_{N_x,N_y} = \begin{cases} \dfrac{\omega\rho_f}{\bar{k}_{N_z}} e^{-i\bar{k}_{N_z}z_1} \cdot \dot{W}_{0;N_x,N_y} & N_x \neq 0 \text{ or } N_y \neq 0 \\ \dfrac{\omega\rho_f}{k_{zo}} e^{-ik_{zo}z_1} \cdot \dot{W}_{0;0,0} - \left(-P_o e^{-i2k_{zo}z_1}\right) & N_x = 0 \text{ and } N_y = 0 \end{cases} \tag{19}$$

$$T_{N_x,N_y} = \frac{\omega\rho_f}{-\bar{k}_{N_z}} e^{i\bar{k}_{N_z}z_2} \cdot \dot{W}_{1;N_x,N_y} \qquad \text{for all } N_x, N_y \tag{20}$$

Generally, the acoustic pressure can be evaluated at any location in the fluid domains by evaluating the double infinite sum. In practice, this evaluation introduces truncation error that is mitigated by including

an increasing number of modes. However, the far-field pressures are characterized by a finite set of discrete modes/angles that radiate, or propagate, into the far-field. The form of the wavenumber component normal to the surface $\bar{k}_{N_z}$ dictates which mode pairs represent supersonic traveling waves that radiate and subsonic components that are range-dependent. The radiating modes satisfy the condition

$$k^2 > \left(\frac{2\pi N_x}{L_x} + k_{xo}\right)^2 + \left(\frac{2\pi N_y}{L_y} + k_{yo}\right)^2, \tag{21}$$

which defines the ellipse of radiating wavenumbers denoted as Λ. The relationship shows that for a given driving frequency ($k = 2\pi f/c$), there is a finite set of structural surface modes that radiate acoustic energy into the far-field. As we sweep through frequency, an increasing number of modes "cut on" and radiate energy. Each cut-on mode represents a redistribution of acoustic energy from specular reflection and transmission into other angles of radiation, which are defined as

$$\theta_{N_x,N_y} = \sin^{-1}\left(\frac{1}{k}\sqrt{\bar{k}_{N_x}^2 + \bar{k}_{N_y}^2}\right) \quad \text{and} \quad \phi_{N_x,N_y} = \tan^{-1}\left(\frac{\bar{k}_{N_y}}{\bar{k}_{N_x}}\right). \tag{22}$$

The modes that fall outside the radiation ellipse represent pressure contributions that exponentially decay in amplitude in the z-direction and are referred to as evanescent, or inhomogeneous, acoustic waves. Therefore, the far-field pressures can be expressed as the finite summations

$$p_{sc}^{rad}(x,y,z) = \sum_{\{N_x,N_y\}\in\Lambda} S_{N_x,N_y}\, e^{i\bar{k}_{N_x}x} e^{i\bar{k}_{N_y}y} e^{i\bar{k}_{N_z}z} \tag{23a}$$

$$p_{t}^{rad}(x,y,z) = \sum_{\{N_x,N_y\}\in\Lambda} T_{N_x,N_y}\, e^{i\bar{k}_{N_x}x} e^{i\bar{k}_{N_y}y} e^{-i\bar{k}_{N_z}z}. \tag{23b}$$

The implementation of this Fourier analysis for wave field extrapolation is verified with numerical examples in the following section.

5. NUMERICAL RESULTS

As a verification of the far-field pressures determined by the Fourier analysis, several material and geometric configurations are compared to analytical and numerical models. These configurations include both homogeneous elastic layers as well as elastic substrates with cylindrical substructures. The Fourier approach is based on knowledge of the surface elastic response, which is determined numerically. A discussion of this computational setup follows. All the first-principles computations presented here are done with the *hp-finite-element* solver STARS3D described in [13]. All the needed three-dimensional computational models are generated using the geometry and mesh generation platform Capstone [14].

The generalized elastic unit cell domain used in this study is depicted in Fig. 2, and the dimensions of the unit cell are available in Table 1. This geometry allows for the introduction of a cylindrical inclusion Ω_v centered in the middle elastic layer Ω_2, as well as up to three elastic layers of differing materials. When the material properties of Ω_1, Ω_2, Ω_3, and Ω_v are defined to be equivalent, the unit cell of an isotropic elastic

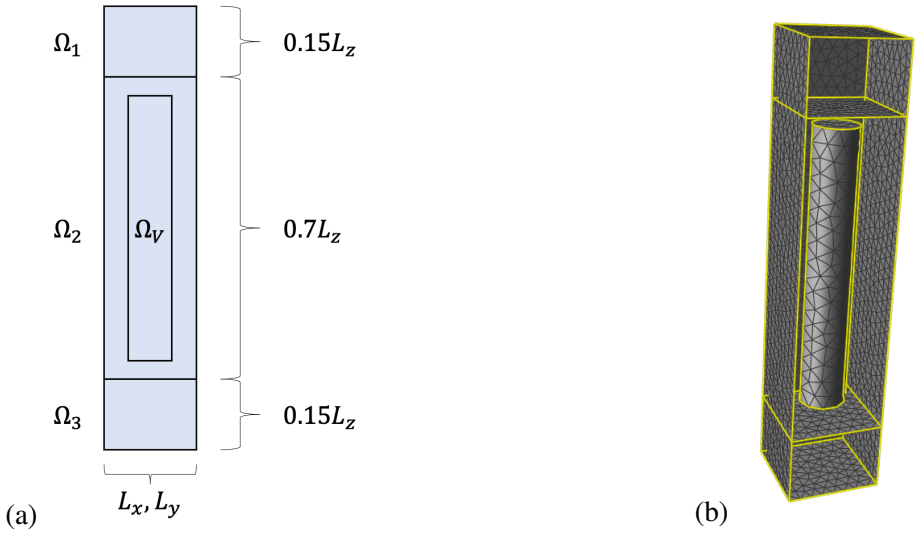

Fig. 2—Elastic unit cell (a) domain description (b) computational model generated with Capstone

Table 1—Dimensions of the Elastic Unit Cell, Cylindrical Inclusion, and Fluid Domains

Parameter	Length (10^{-3}m)
Lx	2.000
Ly	2.000
Lz	9.525
Cylinder Radius	0.500
Cylinder Length	6.000
F_L	1.500
D_L	10.000

plate is recovered. The materials considered in this study are steel and nylon, and both fluid domains are treated as water. In Table 2, the elastic and fluid properties are listed. Also shown in Fig. 2 is the mesh model of the generalized unit cell that is used in the finite element analysis. Note that the fluid domains are not shown in Fig. 2. In order to model the infinite extent of the bounding fluids, a perfectly matched layer (PML) is introduced on either side of the unit cell. The PML ensures that the pressure field of the fluid domains consists exclusively of outgoing waves and thus enforces a radiation condition. As previously demonstrated by Dey et al., the PML approximation suffers from consistency issues when the fluid-elastic interface intersects the PML regions [15]. In order to arrange that the PML domain does not coincide with an interface modeled by differing governing equations, a fluid region is included between the elastic region and PML. The resulting computational domain is shown in Fig. 3, where the domain Ω_j encompasses the elastic unit cell, the fluid domains Ω_{Fi} are included to avoid consistency issues, and the PML regions Ω_{Di} provide that there are no reflected waves. The surfaces Γ_{EFi} denote the fluid-elastic interfaces where the normal displacement of the plate is evaluated for use in the Fourier analysis and as such are located at $z = z_j = \{z_1, z_2\}$.

Table 2—Elastic and Fluid Properties of the Materials Considered

Elastic Material	Young's Modulus (GPa)	Density (kg/m^3)	Poisson Ratio
Steel	206.85	7694.18	0.30
Nylon	2.86	994.70	0.39
Fluid	**Sound Speed (m/s)**	**Density (kg/m^3)**	
Water	1498.60	1025.98	

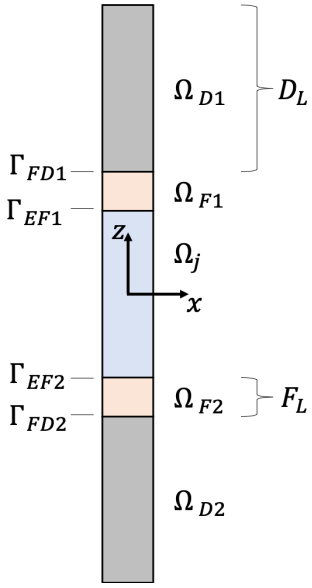

Fig. 3—Computational domain description of the elastic unit cell and corresponding fluid columns

In Fig. 3, the computational domains are drawn to scale for the model used in this study. The dimensions along the normal of the fluid domains F_L and the PML regions D_L, available in Table 1, require some discussion. In the practical application of the Fourier projection, it is expected that the extent F_L of the finite fluid domains will be minimized such that the length is modeled by a single element. This restriction on the size of the finite fluid regions reduces the computational domain and the associated dispersion error [6], while ensuring that the fluid PML domain does not intersect the fluid-structure interface. However, in the current effort to verify the implementation of Fourier analysis, the finite fluid regions are extended to include the "far-field" xy-planes of interest, which are denoted as Γ_{FDi} in Fig. 3. The measure of F_L is chosen to be several acoustic wavelengths for the higher frequencies considered to signify that the pressures on that plane can be considered to be in the far-field of the wet surfaces and an be used for comparison.

The PML approximation implemented in STARS3D is based on the complex-coordinate stretching approach [4, 15]. The outgoing acoustic waves decay exponentially due to the attenuation function in the coordinate transformation to ensure no reflections at the boundary, and as such, the solution within the PML domains have no physical significance. The effectiveness of the PML approximation to enforce the radiation condition is dependent on the amount of attenuation in the layer and therefore the size D_L of the PML regions [16]. As a result, for a fixed attenuation parameter the measure of the PML layer required to certify no significant reflection at the domain truncation is frequency dependent. For this study, the attenuation function and attenuation parameter value follow those given in [16], and as such, the length of the PML

domain was designed so that $kD_L \approx 0.5$ for the longest wavelengths (lower frequencies) in the band of interest. As a rule of thumb to confirm that the outgoing waves are exponentially decaying as they propagate through the PML layer, the modulus of the pressure was probed at the truncation boundary and was verified to be at least three orders of magnitude smaller than the incident pressure.

Using the computational configuration described, we verify the pressures on Γ_{FDi} determined from the Fourier analysis of the elastic motion evaluated at the fluid-structure interfaces. Three substrate material configurations are considered with and without periodic inclusions: a steel plate, a nylon plate, and a steel-nylon-steel (SNS) multilayered substrate with material thicknesses shown in Fig. 2.

5.1 Homogeneous Unit Cells

The Fourier analysis first is verified with the well-studied configurations of isotropic multilayered semi-infinite plates forced by an obliquely incident plane wave. An excellent review of multilayer modeling based on the theory of elasticity with matrix techniques is presented by Lowe [17], and the Global Matrix formulation has been used here as an analytical solution for the reflected and transmitted plane waves. These unit cells are homogeneous in the plane of infinite periodicity, and as such, the scattering of the incident plane wave is defined by specular reflection and transmission at a single angle based on Snell's Law [12]. Therefore, the far-field pressures determined by the Fourier analysis also describe the pressures at the fluid-structure interfaces. Without loss of generality, the pressure wave is defined as obliquely incident with $\theta_o = 60^\circ$ and $\phi_o = 0^\circ$, so that the forcing and resulting structural-acoustic response is invariant in the y-direction.

In the figures that follow, the scattered and transmitted pressures are shown in different plots. There are three data sets shown in each plot: the pressure predicted analytically for the homogeneous elastic layers, the pressures computed by STARS3D on the fluid-structure interfaces, and the far-field pressure evaluated at Γ_{FDi} with the Fourier analysis. These plots show excellent agreement between the three methods of determining the fluid pressures. The importance of properly sizing the PML regions is also referenced, as is evident by the breakdown of the numerical model at the lowest frequencies. The PML was designed for a minimum frequency of 10 kHz and was used for the entire frequency range shown. As such, at the lowest frequencies, the current PML region does not establish the absence of reflected waves at the truncation boundary and a resizing of the PML extent is required. In Fig. 4, it is clear that for the given thickness of the plate, the steel layer appears to be acoustically rigid for most of the frequency range considered. This is contrast to the response of the nylon plate in Fig. 5, which is characterized by less of an impedance mismatch with the coupled fluids. The SNS multilayered substrate in effect "softens" the steel plate by replacing the core of the plate with a compliant material, resulting in a more dynamic frequency response.

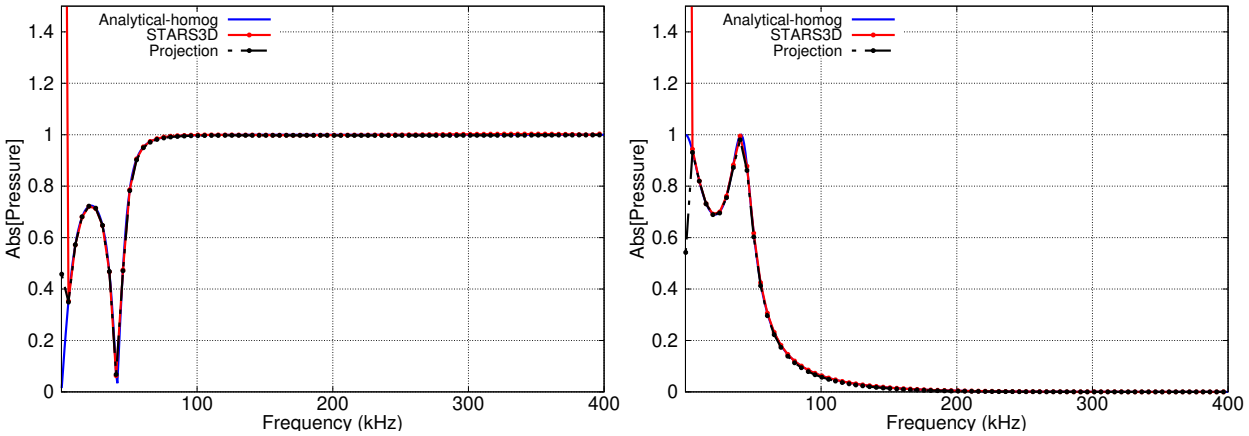

Fig. 4—Scattering (left) and transmission (right) from a steel plate

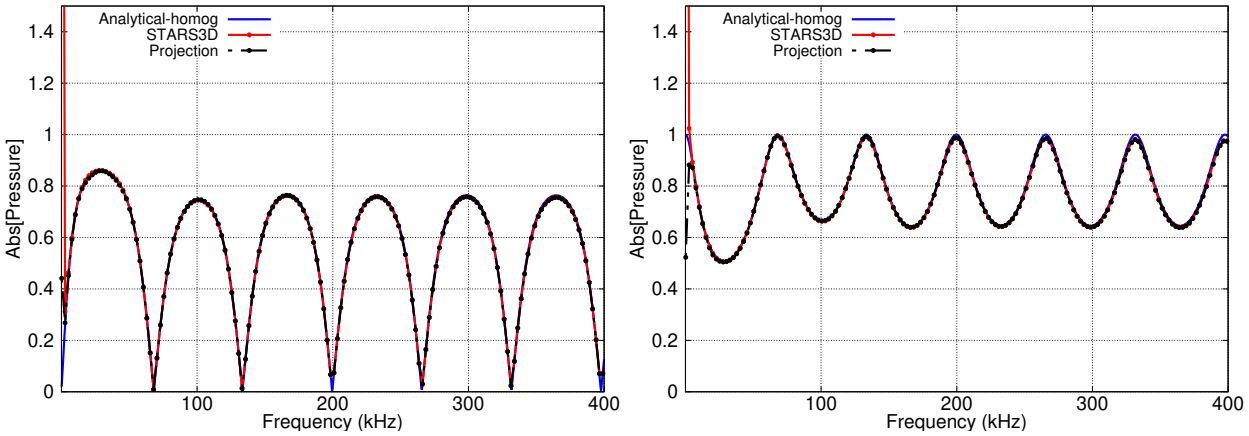

Fig. 5—Scattering (left) and transmission (right) from a nylon plate

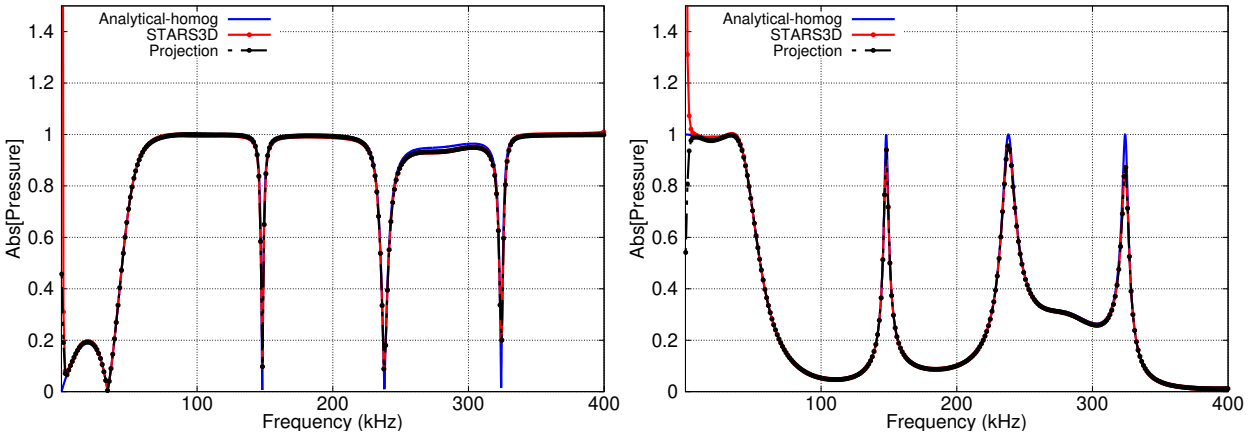

Fig. 6—Scattering (left) and transmission (right) from a multilayered substrate (SNS)

5.2 Periodic Cylindrical Inhomogeneity

To demonstrate that the Fourier analysis is a general methodology not limited to assemblies of isotropic elastic layers, a cylindrical inhomogeneity is introduced in the middle elastic layer such that the material properties of Ω_2 differ from those in Ω_v. The elastic unit cell with the geometric substructure now represents a doubly periodic array of cylindrical discontinuities, with spacing Lx and Ly in an infinite elastic substrate. In Figs.7-10 below, the substructure is introduced into the homogeneous nylon substrate and the multilayered SNS substrate. We consider two configurations for Ω_v, first as a cylindrical void modeled as a vacuum, and as a suspended steel rod. For each configuration, the scattering response is shown for two planar waves with differing angles of incidence. The first planar wave is the same as that considered with the homogeneous unit cells with $\theta_o = 60°$ and $\phi_o = 0°$. The second planar wave $\theta_o = 60°$ and $\phi_o = 45°$ for truly 3D oblique incidence.

The reverberation of elastic substructures excites a full spectrum of structural waves in the unit cell. The resulting presence of both acoustically evanescent and propagating surface waves at the fluid-structure interface by definition means that the pressure on the fluid-structure interface is no longer equivalent to the far-field pressures as was the case of the isotropic single and multilayered plates [7]. Therefore, the far-field pressures predicted by the Fourier analysis are compared to the pressures predicted by STARS3D at the far-side plane of the physically meaningful finite fluid domains Γ_{FDi}. In the following figures, the analytical solution for the analogous homogeneous configuration is replicated to highlight the effect of the internal structure on the far-field acoustic response.

These figures demonstrate that the Fourier analysis shows excellent agreement with the far-field pressures predicted by the finite element analysis for substrates with doubly periodic elastic inclusions. The figures also suggest that at the lower frequencies, the influence of the periodic inhomogeneities can presumably be analyzed in the framework of static homogenization, however the presence of sharp resonances at the higher end of the frequency band suggests that we have begun to excite the local resonances of the internal structures. Interestingly, in the frequency range considered, the angles of reflection and transmission from the elastic media are still dictated by Snell's Law. That is, there is only one mode of propagation into the far-field and it is the same mode, $N_x = N_y = 0$, as for the isotropic layer configurations, and yet the frequency dependence of the reflection and transmission is altered considerably. In the framework of the previous Fourier analysis discussion, this can be interpreted partially as a redistribution of the structural energy into other harmonics that couple to evanescent acoustic waves. The presence of only a single radiation mode means that the mean-squared pressure, or acoustic intensity, is spatially invariant in the far-field; the magnitude of the pressure at a single point in the far-field describes the magnitude of the pressure anywhere in the far-field. In order to induce more modes of radiation, the driving frequency must be increased. Considering Eq. (21) with the parameter values of this study and the planar wave with incidence angles $\theta_o = 60°$ and $\phi_o = 0°$, the next mode of radiation does not cut on until outside the frequency range considered:

$$f_{c1} = \frac{ck_{c1}}{2\pi} = -\frac{2\pi N_x}{L_x(\sin\theta + 1)}\frac{c}{2\pi} \approx 402 \text{ kHz}. \tag{24}$$

Further increasing the frequency will decrease the relevant wavelength so that the elastic response of the internal resonators becomes appreciable and redistributes elastic spectral content to surface modes that radiate acoustic energy into the far-field. That is the physical reasoning for why increasing the frequency results in more complex far-field radiation patterns. In the absence of internal resonators, as in the isotropic

elastic layers considered, the higher-order radiation modes will cut on at the same frequencies but the modal content for those modes will remain null, thus maintaining the angles of reflection and transmission defined by Snell's Law.

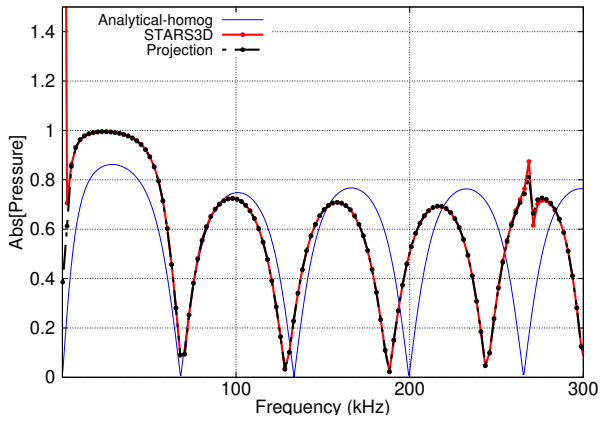

(a) $\theta_o = 60°$ and $\phi_o = 0°$

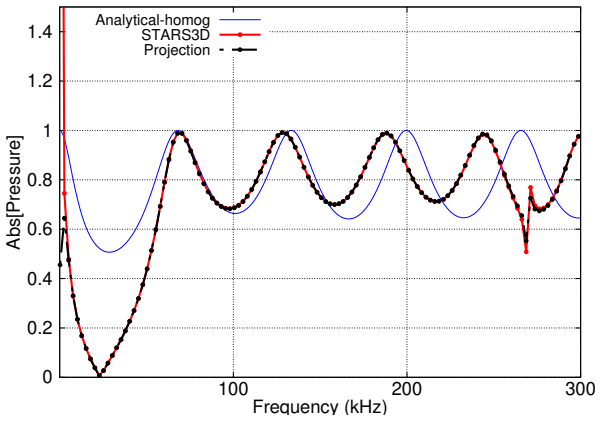

(b) $\theta_o = 60°$ and $\phi_o = 0°$

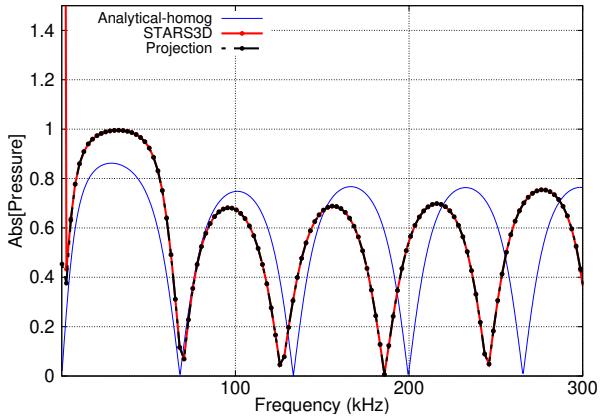

(c) $\theta_o = 60°$ and $\phi_o = 45°$

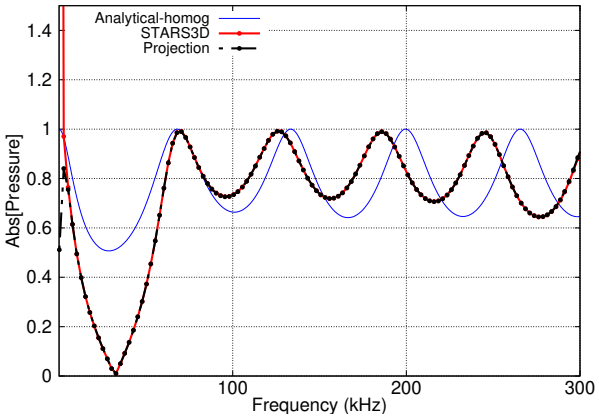

(d) $\theta_o = 60°$ and $\phi_o = 45°$

Fig. 7—Scattering (left) and transmission (right) from a nylon substrate with periodic voids

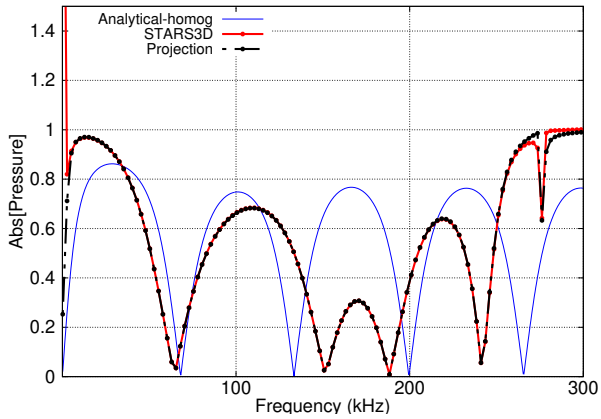

(a) $\theta_o = 60°$ and $\phi_o = 0°$

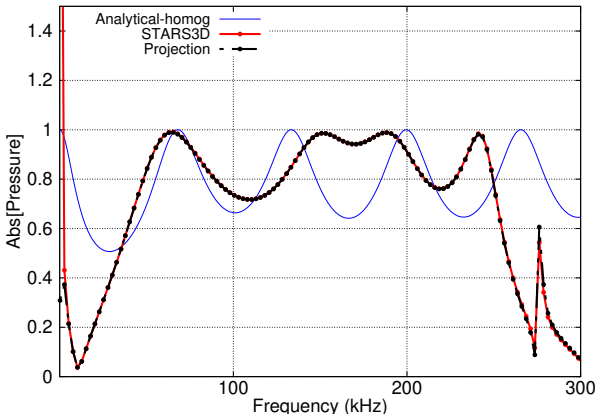

(b) $\theta_o = 60°$ and $\phi_o = 0°$

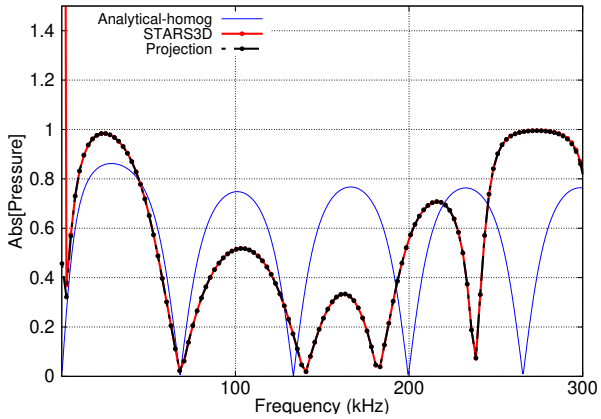

(c) $\theta_o = 60°$ and $\phi_o = 45°$

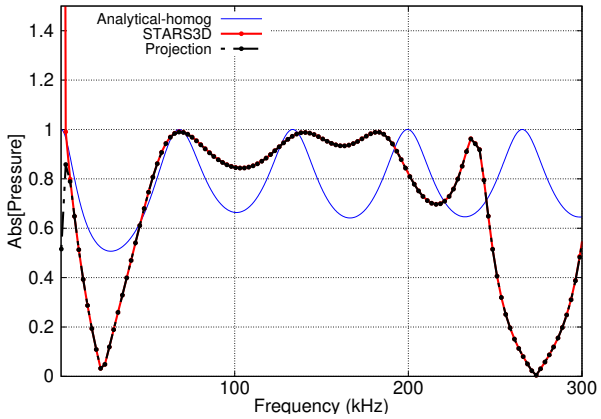

(d) $\theta_o = 60°$ and $\phi_o = 45°$

Fig. 8—Scattering (left) and transmission (right) from a nylon substrate with periodic steel inclusions

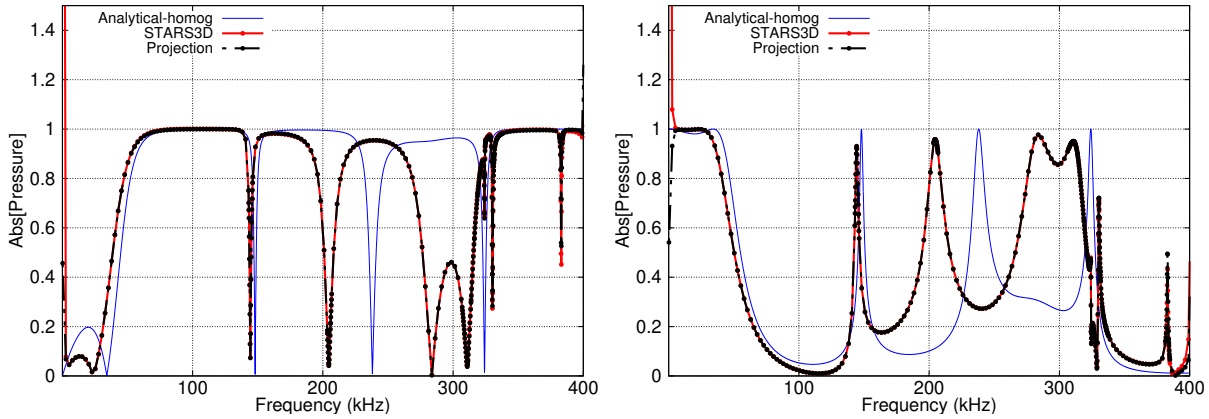

(a) $\theta_o = 60°$ and $\phi_o = 0°$

(b) $\theta_o = 60°$ and $\phi_o = 0°$

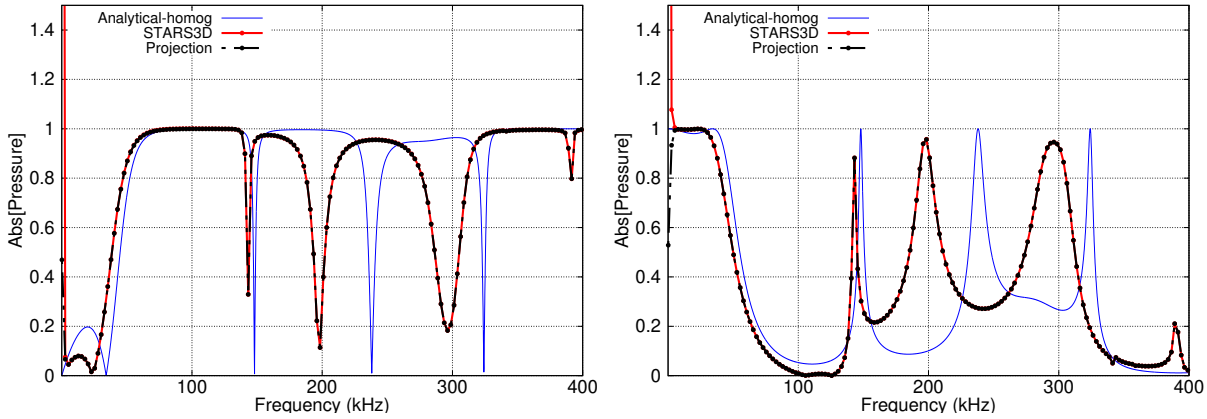

(c) $\theta_o = 60°$ and $\phi_o = 45°$

(d) $\theta_o = 60°$ and $\phi_o = 45°$

Fig. 9—Scattering (left) and transmission (right) from a SNS substrate with periodic voids

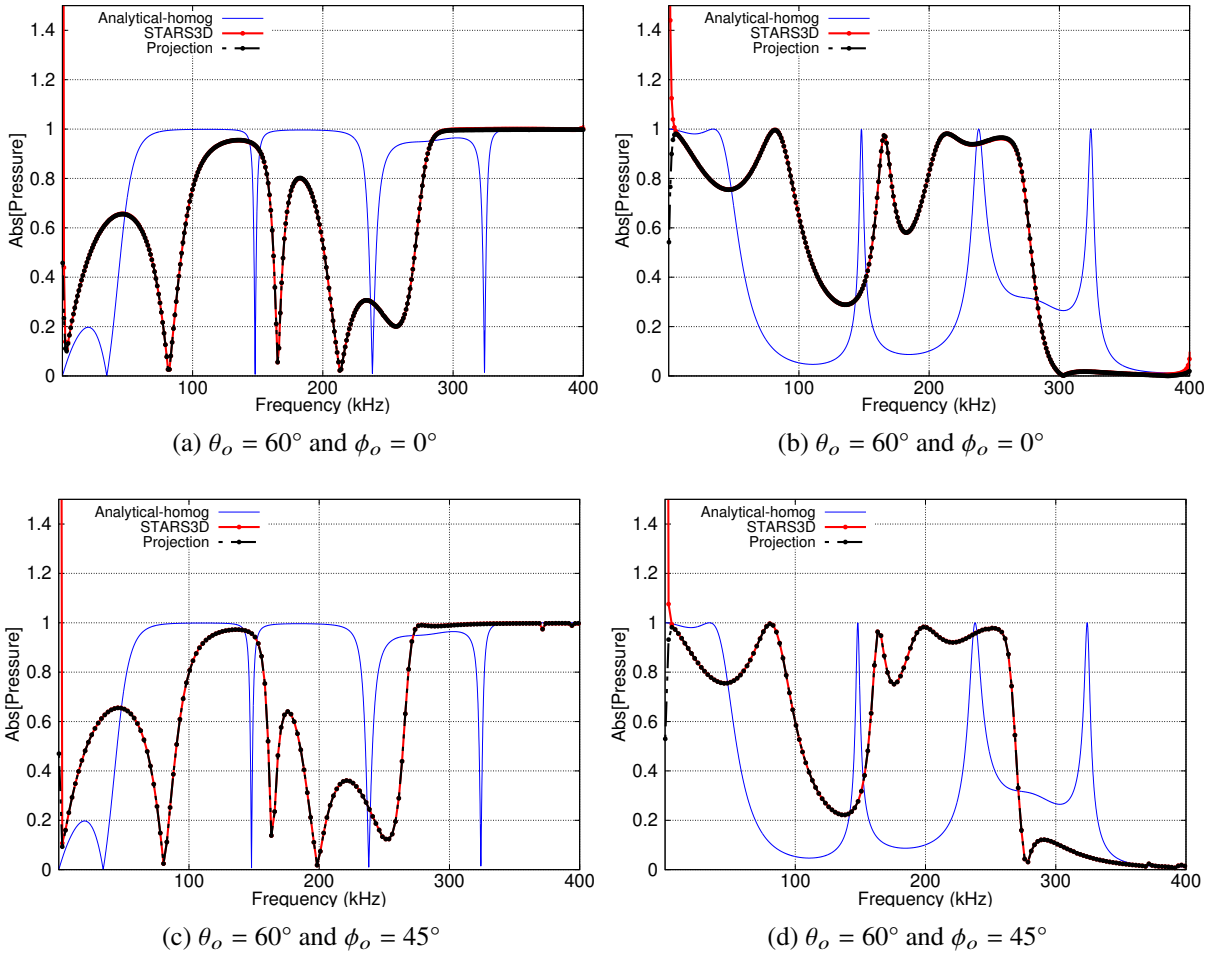

(a) $\theta_o = 60°$ and $\phi_o = 0°$

(b) $\theta_o = 60°$ and $\phi_o = 0°$

(c) $\theta_o = 60°$ and $\phi_o = 45°$

(d) $\theta_o = 60°$ and $\phi_o = 45°$

Fig. 10—Scattering (left) and transmission (right) from a SNS substrate with periodic steel inclusions

6. CONCLUSIONS

We have described a Fourier analysis that predicts the scattered and transmitted far-field pressures from the transverse surface motion of doubly periodic elastic panels. It was demonstrated that this extrapolation analysis can be used to accurately predict radiation fields for multilayered elastic media with periodic complex internal structures from the analysis of a single unit cell. In addition to only requiring the elastic response of a single unit, this analysis forgoes the need to discretize the fluid domains into the far-field, thus reducing the associated computational expense. One of the secondary benefits of this projection method is that it does not require any modifications of existing FEM algorithms, but rather can be carried out externally from existing computational infrastructure as was done in this study with results from STARS3D.

Of immediate interest is the application of the Fourier analysis to include subsequent cut-on modes that result in additional angles of radiation. The existence of additional radiation modes occurs at higher frequencies, and thus will manifest as a result of the reverberation of elastic waves from the periodic substructures and the corresponding elastic resonances. Another potential extension of the Fourier analysis would be to retain increasing numbers of evanescent modal components in order to describe the range-dependent pressure fields, including the surface pressures at the fluid-structure interfaces. Formally, the complete spectrum of Fourier components is required to describe the surface pressures, but it may be possible to exploit deceasing modal amplitudes to truncate the series effectively while maintaining sufficient accuracy of the field description. For use with more complex configurations at high frequencies, the design of the computational domains associated with the unit cell will necessitate some optimization to reduce the degrees of freedom of the numerical analysis. As such, further implementation of algorithmic strategies to size the PML regions dynamically as a function of frequency should be pursued. Additionally, comparison with experimental measurements of the scattering from periodic media is required to validate the Fourier analysis presented.

When evaluating the impact of using such panel material on large structures, one needs to obtain a *homogenized* representation [18]. Most of the homogenization is for near-field response. We plan to use the far-field projection technique to enable homogenization of such structures for their far-field response.

REFERENCES

1. Z. Liu, "Locally Resonant Sonic Materials," *Science* **289**(5485), 1734–1736 (Sept. 2000).

2. S. Zhang, L. Yin, and N. Fang, "Focusing Ultrasound with an Acoustic Metamaterial Network," *Physical Review Letters* **102**(194301), 1–4 (May 2009).

3. H. Peng and P. F. Pai, "Acoustic metamaterial plates for elastic wave absorption and structural vibration suppresion," *Int. J. Mech. Sci.* **89**, 350–361 (2014).

4. S. Dey and J. J. Shirron, "Computation of Acoustic Transmission Loss Through Doubly-Periodic 3D Elastic Panels," Proceedings of the Noise Control and Acoustics, Chicago, Illinois, USA (ASMEDC), Jan. 2006, pp. 19–23.

5. L. M. Brekhovskikh and O. Godin, *Acoustics of Layered Media I* (Springer Verlag, Berlin Heidelberg, Germany, 1990).

6. S. Dey, J. J. Shirron, and L. S. Couchman, "Mid-frequency structural acoustic and vibration analysis in arbitrary, curved three-dimensional domains," *Computers & Structures* **79**(6), 617–629 (Feb. 2001).

7. E. G. Williams, *Fourier Acoustics: Sound Radiation and Nearfield Acoustical Holography* (Academic Press, London, UK, 1999).

8. J. Gazalet, S. Dupont, J. Kastelik, Q. Rolland, and B. Djafari-Rouhani, "A tutorial survey on waves propagating in periodic media: Electronic, photonic and phononic crystals. Perception of the Bloch theorem in both real and Fourier domains," *Wave Motion* **50**(3), 619–654 (Apr. 2013).

9. D. Mead and A. Mallik, "An approximate theory for the sound radiated from a periodic line-supported plate," *Journal of Sound and Vibration* **61**(3), 315–326 (Dec. 1978).

10. B. Mace, "Sound radiation from fluid loaded orthogonally stiffened plates," *Journal of Sound and Vibration* **79**(3), 439–452 (Dec. 1981).

11. "Discrete Fourier Transform (numpy.fft)," `https://docs.scipy.org/doc/numpy/reference/routines.fft.html#module-numpy.fft`.

12. M. C. Junger and D. Feit, *Sound, Structures, and Their Interaction*, 2nd ed. (MIT Press, Cambridge, Mass, 1986).

13. S. Dey, J. J. Shirron, and L. S. Couchman, "Mid-frequency structural acoustic and vibration analysis in arbitrary, curved three-dimensional domains," *Comp. Struc.* **79**, 617–629 (2001).

14. S. Dey, R. A. Aubry, B. K. Karamete, and E. L. Mestreau, "Capstone: A geometry-centric platform to enable physics-based simulation and system design," *IEEE Comp. Sc. Eng.* **18**(1), 32–39 (Jan-Feb 2016).

15. S. Dey, W. Szymczak, A. Sarkissian, and J. Bucaro, "Scattering from targets in three-dimensional littoral and surf-zone environments with multi-layered elastic sediments based on an interior-transmission formulation," *Computer Methods in Applied Mechanics and Engineering* **260**, 24–39 (June 2013).

16. J. J. Shirron and T. E. Giddings, "A finite element model for acoustic scattering from objects near a fluid–fluid interface," *Computer Methods in Applied Mechanics and Engineering* **196**(1-3), 279–288 (Dec. 2006).

17. M. Lowe, "Matrix techniques for modeling ultrasonic waves in multilayered media," *IEEE Transactions on Ultrasonics, Ferroelectrics and Frequency Control* **42**(4), 525–542 (July 1995).

18. C. F. Sieck, B. Alu, and M. R. Haberman, "Dynamic homogenization of acoustic metamaterials with coupled field response," *Physics Procedia* **70**, 275–278 (2015).